Hindawi
Journal of Engineering
Volume 2022, Article ID 8386877, 10 pages
https://doi.org/10.1155/2022/8386877

Research Article

Analysis of Crashworthiness of Bishoftu Pickup Vehicle Structure during Side Pole Crash

Adane Gashu[1] and Ramesh Babu Nallamothu[2]

[1]*Bahir Dar Institute of Technology, Bahir Dar University, Bahirdar, Ethiopia*
[2]*Department of Mechanical Engineering, SoMCME, ASTU, Adama, Ethiopia*

Correspondence should be addressed to Ramesh Babu Nallamothu; rbnallamothu@gmail.com

Received 21 May 2022; Revised 20 November 2022; Accepted 6 December 2022; Published 22 December 2022

Academic Editor: Paolo Castaldo

Now a day's, vehicle accident is becoming a critical issue all over the world, especially in Ethiopia. These vehicles have not been checked for any crash safety test specifications and are not evaluated for crashworthiness. So, it is now time to consider the safety features of Bishoftu pickup vehicles (BPV) to reduce the grave consequences for their users. This paper aimed to improve the crashworthiness of the existing Bishoftu pickup vehicle through remodeling. The structural response to a frontal collision with an existing BPV is analyzed. Based on the results obtained from the existing model, modifications are made by means of energy-absorbing components, a stable frame structure, and better crash performance. For doing the analysis software like CATIA is used for 3D modeling, and LS-DYNA is used for FEM analysis. The results show that by applying the modification, 39 kN (7.82%) of impact force is reduced and 5 kJ (3.52%) of additional energy is absorbed during the frontal collision. Finally, it can be concluded that with the modified model, the safety and crashworthiness of the BPV were greatly improved without affecting the appearance and weight of the existing one.

1. Introduction

The WHO Global Status Report on Traffic Safety for 2018 estimates that 1.35 million people globally perished in road accidents in 2016. With 18.2 deaths per 100,000 people, road accidents are the eighth most common cause of death in the world and the number one killer of kids and teenagers aged 5 to 29. Road fatalities and injuries are distributed equally around the globe, with 93% of deaths taking place in low- and middle-income nations, which account for 41% of all automobiles. About 29% of these deaths are four-wheel drive, 23% are pedestrian, and 3% are cycling [1].

Every country rates car-side crashes as high. Due to the insufficient room for significant deformation during a collision, protecting passengers is particularly difficult, making side impacts very risky. In the USA, side impact incidents continue to rank second after frontal collisions in terms of mortality causes for collision-related cars [2]. The most dangerous collision is always one in which a car collides with a pole or tree on the side. According to statistics, the death rate on the trackside while a strong pole was present increased by 52% between 2004 and 2009. In that situation, the percentage of side effects exceeds 60% [3].

To quantify side impacts, a lot of research has been done on the lateral structure of automotive energy absorption and human reactions in the case of a side impact [4]. This study employs the finite element approach to examine the dynamic properties of a pickup truck made in Bishoftu, Ethiopia, when it collides with a side post. Figure 1 depicts a Bishoftu pickup truck (BPV). They are generally double-capped with four wheels (two on the front and two on the rear). It contains five occupants: the driver generally sits on the front left side of the cabin, one on the right, three on the rear part of the cabin, and there is also a luggage compartment on the rear part of the vehicle. It has a maximum velocity of 120 km/hr, and the gross vehicle weight (including vehicle and occupant) is around 2495 kg.

Figure 1: Bishoftu pickup structure.

The automotive industry's top concerns for ever-increasing standards in fuel efficiency and crash safety have been lightweight vehicles and structural crashworthiness. Like cars, which are designed to have high speeds and be lightweight, road accidents and injuries are rising dramatically. One of the most important factors is assessing vehicle safety [5]. However, these two options are frequently in opposition to one another, necessitating trade-offs to ensure that the vehicle structure can withstand crashes with the greatest amount of force while maintaining the integrity of the passenger compartment for the safety of the passenger [6–9].

The side-impact and protection measures did not attract much attention from researchers as frontal impact, for reducing injuries caused by side crashes of BPV with poles or trees. The goal of this research was to address and enhance the side crashworthiness of the current BPV. Therefore, the modeling and analysis of the current BPV structure were the first tasks completed in this research. The construction of the current BPV (Bishoftu pickup vehicle) was changed based on how the results were interpreted. Modeling for this assignment was carried out using CATIA v5 software, while FEA analysis was carried out using LS-DYNA.

1.1. Side Impact. In an effort to decrease the number of injuries and fatalities among vehicle occupants following a side accident, there are numerous vehicle crash test regulations that support vehicle manufacturers in improving the safety of their vehicle products. In 1990, the Federal Motor Vehicle Safety Standards started incorporating the present requirements, including the standard for side impact protection (FMVSS) 214. Additionally, the National Highway Traffic Safety Administration (NHTSA) established a moving deformable barrier (MDB) in 1997 for testing crashes involving side impacts. Figure 2(a) shows the collision between a 1,368 kg MDB driving at 54 km/h with a crabbed wheel angle of 27° and a stationary vehicle at a 90° angle. The height of the deforming portion of the barrier is 828 mm as measured from the ground [10]. This aid in determining what may occur if a car sideswiped another at an intersection. The Insurance Institute for Highway Safety (IIHS) begins testing vehicle side impact using modified MDB in 2003, as shown in Figure 2(b). A modified MDB weighing 1500 kg travels at 50 km/h in this test before colliding with the driver's side of a stopped vehicle. A typical midsize SUV is the same size as the IIHS MDB [11].

Understanding the effects of a car swerving off the road and colliding with a utility pole is made easier by this test's simulation. As seen in Figure 3, the NCAP side pole test involves driving a vehicle against a fixed, rigid pole measuring 254 mm (10 inches) in diameter at a speed of 32 km/h (20 mph).

Studies on BPV are scarce. The strength of the BPV's structure was evaluated using FEA software in rollover static impact, rear, front, and side impacts. A modified model of BPV was constructed by incorporating numerous alterations to the structure based on the data obtained from the current model. Despite the fact that the dynamic crash event involving the dummy inside the automobile was not examined, the study effort's findings showed that the updated model is much better than the previous model.

The procedures used to undertake the analysis and predict the side crashworthiness of the Bishoftu pickup vehicle are shown in Figure 4.

1.2. Modelling. The pickup geometry in Bishoftu, the car's manual, and specifications gathered during data collection are used to model the vehicle [12]. The pieces were modeled individually and combined in CATIA. The primary sections that were simulated were the front, side, roof, and back body structures; the chassis; the steering; the windshield; and the front and rear tires. The combined 3D modeling of those structures is displayed in Figure 5.

1.3. Mesh. When examining the BPV's construction, a shell element is used to represent the principal components because their thickness is significantly less than their length and breadth. As a result, the auto mesh type was used. The LS-DYNA program was used to mesh the vehicle geometry by combining linear, quadrilateral, and triangular components. For the entire model, the element size ranges from 4 to 8 millimeters. The mesh model has 907608 nodes, 15848 solid components, and 862079 shell components. Figure 6 shows the BPV that has been meshing.

1.4. Material Properties and Thicknesses. Materials for car components are chosen from the LS-DYNA material catalog. The tire's keyword was created using Mat Elastic modeling software, while Mat Piecewise Linear Plasticity was used to model the vehicle's chassis and windshield. Axles and engine components are two examples of items that were modeled using Mat Rigid since they are not prone to deformation. The mechanical properties and shell thickness of the vehicle component are detailed in Tables 1 and 2.

Most car parts have a section shell used to define their thickness, whereas the remaining parts have a solid element. The thickness value for shell components is computed using the density and mass values from the aforementioned data sources.

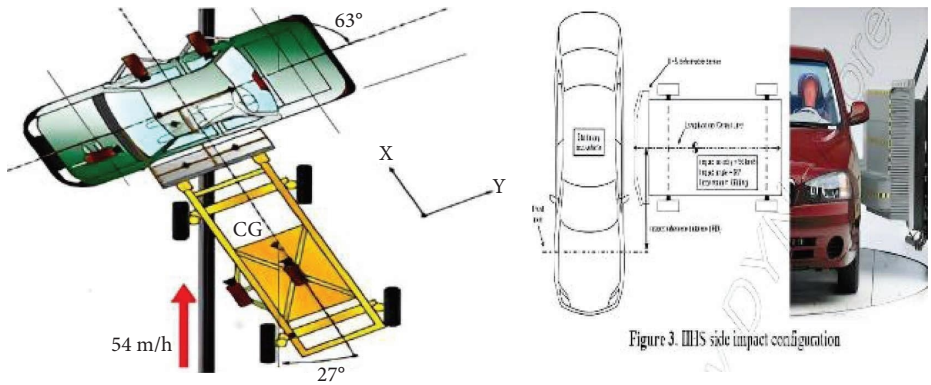

(a) (b)

Figure 2: (a) FMVSS side impact test (b) IIHS side-impact configuration.

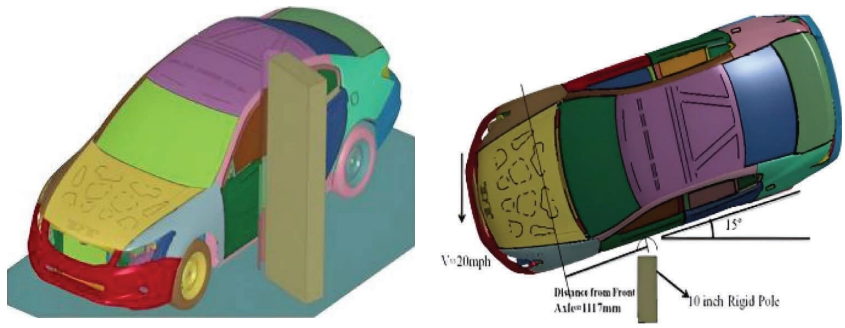

(a) (b)

Figure 3: NACP side impact.

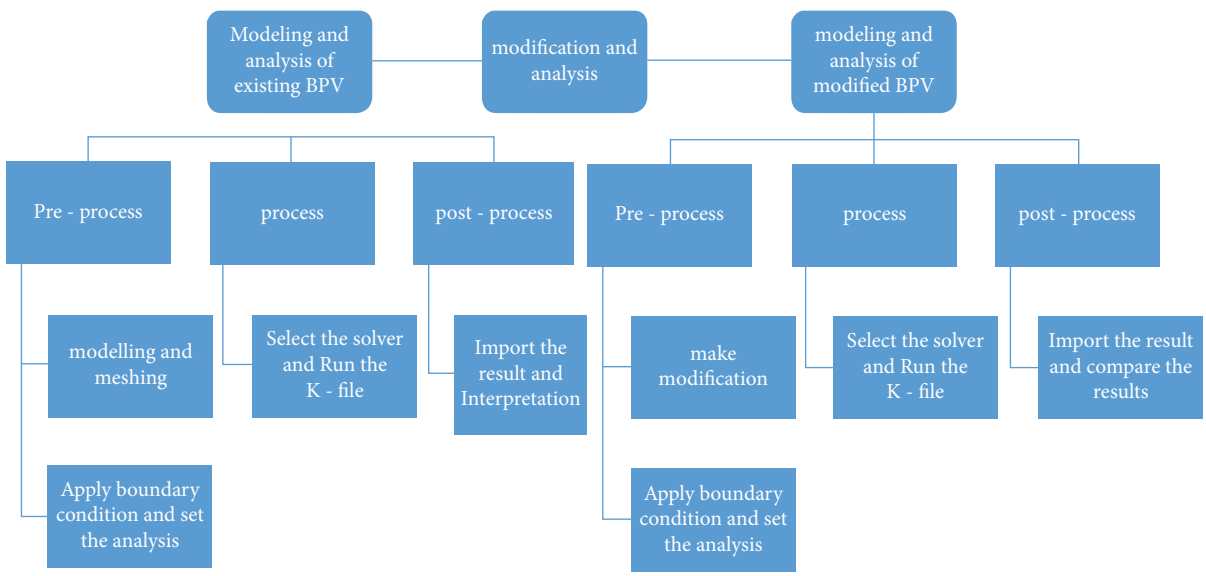

Figure 4: FEA.

1.5. Constraint Definition. These interactions regulate the transmission of forces and moments between individual members and are specified between the surfaces of various parts. Different components of the vehicle have kinematic joints defined for them. In LS-DYNA, the constraint between two deformable parts was given by the keyword

Figure 5: A 3D model of BPV.

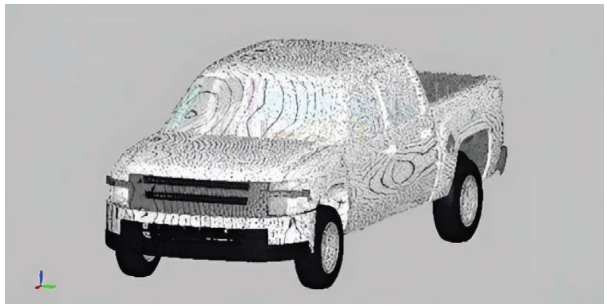

Figure 6: Meshed BPV.

Table 1: Mechanical properties of a vehicle component.

Vehicle item	Mass density (kg/m^3)	Young's modulus (Pa)	Poisson's ratio	Yield stress (Pa)	Tangent modulus
Vehicle structure	7890	$1.87e+11$	0.28	$2.45e+8$	$1e+09$
Chassis	7850	$2e+11$	0.26	$3.45e+8$	
Windscreen	3150	$7.39e+10$	0.22	$1.380e+08$	$1e+09$
Tire	1510	$3.00e+09$	0.45		

Table 2: Thicknesses.

Components	Thicknesses (mm)
Vehicle structure	0.94
Chassis	4
Windscreen	4
Tire	7

Table 3: Contact between different parts of BPV.

Contact	Slave	Master
Surface to surface	Tire	Ground
Surface to surface	BPV	Pole
Single surface	Whole vehicle	Non

CONSTRAINED_NODAL_RIGID_BODY in entity creation. Also, to connect a rigid body to a deformable body, CONSTRAINED_EXTRA_NODE_SET is used and constrained RIGID BODIES is another keyword used to connect rigid bodies with another rigid body. In addition, JOINT_REVOLUTE was used to constrain the tire with the vehicle components.

1.6. Contact Definition. To avoid penetration during the accident, contact between the two sections is provided. The keyword manager offers a wide variety of contact types. Table 3 lists the many contact types that were employed in this work.

1.7. Components Missing and Simplification. All the passenger dummies and other vehicle components were not modeled in order to reduce the length of the computer simulation. However, the center of gravity is determined, and the total of the passengers' and BPV's mass is applied at that location when taking that into account.

1.8. Boundary Condition. To examine the real crash event of a BPV impacting a post or tree, an FEA model is constructed in which the vehicle travels at a speed of 32 km/h and strikes the rigid pole at an angle of 75 degrees with the vehicle's longitudinal axis shifted. The stiff pole utilized in the simulation can be obtained from [13, 14]. The stiff pole has a

254 mm diameter and is 2150 mm long when placed vertically.

The pole is always aligned with the center of gravity (CG) of the driver's head because of the way the car is moving [15]. Figures 7(a) and 7(b) depict the LS-DYNA configuration of the BPV model for the side crashworthiness test in accordance with NACP regulations.

1.9. Modification on the Existing Bishoftu Pickup Vehicle. The first thing to consider when making the modification is that the occupants should be extensively protected from direct contact with obstructions and free from an uncontrolled flight. To achieve this goal, the car's body structure is also designed to be as safe as possible, with some crashing zones to absorb energy but also a stiff protective cell for the occupants. Also, it should highly consider the lightweight design criteria. Deformable side beam components are positioned at the BPV frame structure to reduce intrusion into the compartments and the force of impact communicated to the passengers. Figure 8 depicts the site where the modification was installed. The material used for the beam element was designed to act as a bumper and is designed in such a way that it is capable of deformation, together with other linkages. The modification includes material and thickness optimization.

1.10. Side Door Beam Design. The side door beam is one of the essential safety components that fortifies the BPV's side members and helps to lessen the degree of injuries to passengers in a side accident. Under this section, a side door beam with Advanced high-strength steels (AHSS) Docol 1200 DP Steel material is designed for different thicknesses. The various thicknesses are used based on the stable frame structure concept. Excessive modifications can affect the road handling of the vehicles, such as by distracting from the original vehicle's stability, increasing fuel consumption due to the addition of too much weight, and violating other safety regulations, which may result in a violation of the law. So, the new model has the same fuel consumption as the existing BPV because the total mass of the new model is the same as the existing one because of the use of lightweight material.

A HAT cross-section is used for the side door beam, which has high bending resistance with bi-axial bending. The properties, which are summarized in Table 4, will be used directly as physical parameters in LS-DYNA material cards.

1.11. Material, Thickness, and Boundary. MAT_ PIECEWISE_ LINEAR_ PLASTICITY is the material keyword used to specify the material. A shell section is employed to model the side door beam since its thickness is thought to be extremely smally in comparison to its whole length. Elform = 2 is the element formulation for the shell components (Belytschko-Tsay elements). LS-user DYNA's input card ∗ SECTION SHELL/ TSHELL [16], can be used to modify this. To determine how thickness affects the side door beam system's ability to withstand

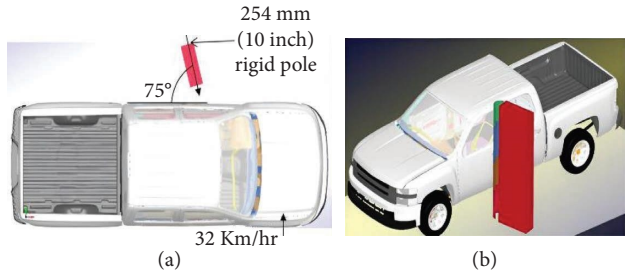

Figure 7: Side test set up.

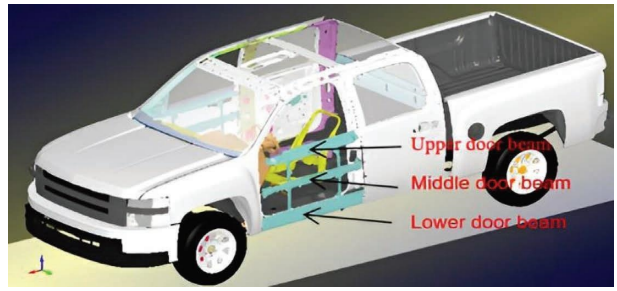

Figure 8: Modified BPV.

Table 4: Side beam material property.

Properties	Units	Value
Mass density, ρ	kg/m^3	7870
Young's modulus, E	Pa	$2.07e+11$
Poisson's ratio, PR	—	0.3
Yield strength (stress), YS	Pa	$1.07e+9$
Ultimate tensile strength, UTS	Pa	$1.22e+9$
Uniform elongation, ε	%	3.9
MARTENSITE	%	95
Elongation at break	%	≥4

impacts, high-strength steel side door beam HAT cross-sections with various thicknesses are taken into account.

There are many factors to be considered during thickness optimization; some of the main factors are as follows:

(i) The ability of the system to absorb shocks or impacts.

(ii) To withstand hits at high speeds.

(iii) Weight, manufacturing process capability, and cost are further design-phase considerations.

In doing so, the side door beam's thickness of 0.886, 1, 1.25, 1.5, 1.7, and 2 mm was taken into consideration. Starting at 0.886 mm thick was chosen because, when the material thickness was lower, it manifested some kind of failure mode. Also, thickness influences the intrusion into the occupant; this leads to masses increases, which will affect fuel consumption because most of the fuel consumption (75%) is due to the weight of the vehicle. So, all this should be taken into consideration when thickness optimization takes place.

The best material thickness among those stated is selected based on variable such as load bearing capacity, stress energy absorption capacity, and decrease in displacement.

The configurations utilized and the boundary conditions are detailed. The test is made up of three parts: the supports (colored red), side door beams (colored blue), and stiff poles (yellow). A stiff body is used to represent the pole, and shell components are used to discretize it. It is more effective to simulate the side door beam and its supports using a single layer of shell components because the thickness of the beam is significantly less than the other dimensions. The components, which have 11,525 elements and 12,780 nodes, are entirely made up of quadrilateral elements. Mat 20 (mat-rigid) is used to represent the rigid pole, while Mat 24 (Mat Piecewise Linear Plasticity) is used for the supports and beams. The test process is the same as the one used for the BPV's complete crash test. The supports were built up or placed in a similar way to how the BPV modification was constructed.

The distance between the side door beam and the side pole was the same as the distance between the BPV and rigid pole. As seen in Figure 9, the support and side door beam collided with the rigid pole while traveling at 32 km/h. All of the degrees of freedom for the stiff pole are fixed (DOFs = 0). The moving beam and its supports are fixed in each DOF, with the exception of the direction of movement.

2. Result and Discussion

2.1. Deformation of Beams. The relative displacement from two nodes—one at the right or left end of the beam, which is not subject to deformation, and another at the center (center) of the beam, which is used to calculate the deformation values. Using this measurement, the deformation graph value is created using the same nodes between 5496 and 7097 for varied thicknesses of beams. From the figure, the deformations of 0.886, 1, 1.25, 1.5, 1.7, and 2 mm are 29, 27.6, 25.1, 22.7, 21.1, and 16.6 mm, respectively. This does not imply that a thinner beam is always preferable. Because additional deformation increases the likelihood of penetration into the primary compartments of the vehicle, the maximum distortion of the beam decreases, and the rate of fall likewise slows with a thickness increase exceeding 1.25 mm.

2.2. Energy Absorption in Beams. Figure 10 depicts the energy absorption as a function of the door beam's thickness. Figure 10 shows that the energy absorption increases as the beam thickness increases from 0.866 mm to 2 mm and is 30.1, 29.5, 28.8, 27.7, 27, and 26.4 J. As a result, the maximum amount of energy that the beam can absorb declines, and the rate of decline likewise accelerates at 1.25 mm in thickness. On the other hand, as seen in Figure 11, the beam deforms more as a result of its higher energy absorption. The maximum amount of energy that the beam can absorb decreases when its thickness increases.

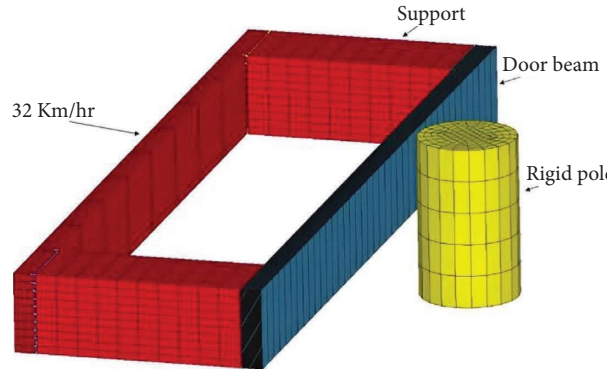

Figure 9: Side pole test.

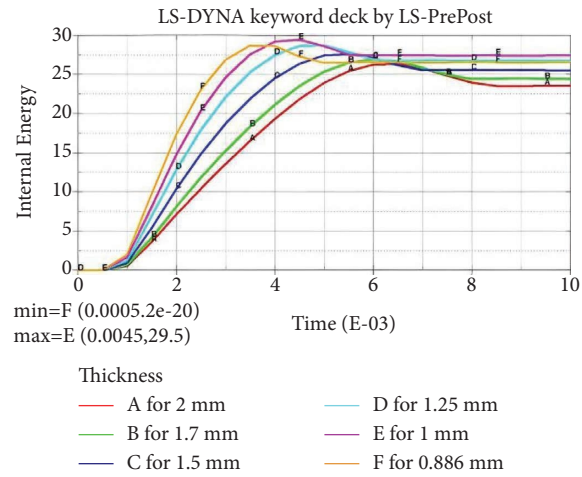

Figure 10: Internal energy with varying thicknesses.

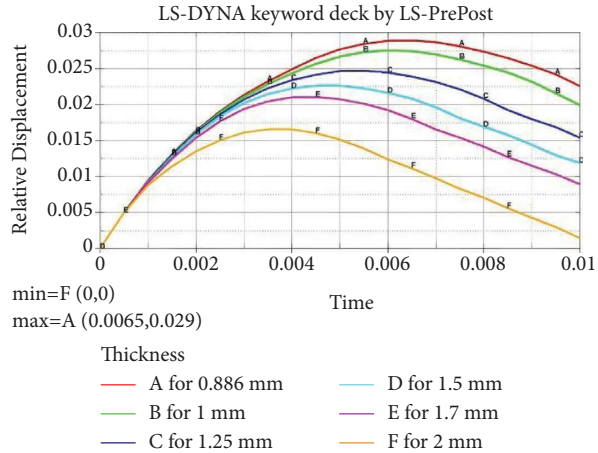

Figure 11: Deformation of different beam thicknesses.

2.3. Impact Force. Although the thickness increases, the maximum impact force between the stiff pole and side door beam also increases. This makes it clear that as the thickness of the beam increases, so does its mass, producing the high

impact force. Also, the results are 1.21, 1.24, 1.34, 1.55, 1.81, and 2.12 kN, respectively, as the thickness increases from 0.886 to 2 mm, as shown in Figure 12. Less thickness is used to raise the load on the beam; thus, this does not mean that a beam with less thickness is preferred. The aforementioned conclusions and observations in the literature can therefore be extrapolated to the conclusion that neither a thinner nor a thicker beam is desirable; rather, it depends on the application [17]. The major goal of this inquiry is to choose a side door beam that is lightweight and has high crash performance without losing impact behavior. From the perspective of impact performance, taking the average value for the stated thicknesses improves the level of performance in comparison to others for the BPV's body sections and passengers. When the thickness of the beam rises above 1.25 mm, both the maximum impact force and the rate increase. Therefore, the door beam with 1.25 mm thickness is better because of its higher energy absorption, less impact force, and relatively the same mass as the existing vehicle model. The chosen beam's van Mosses equivalent stress and displacement graph is shown.

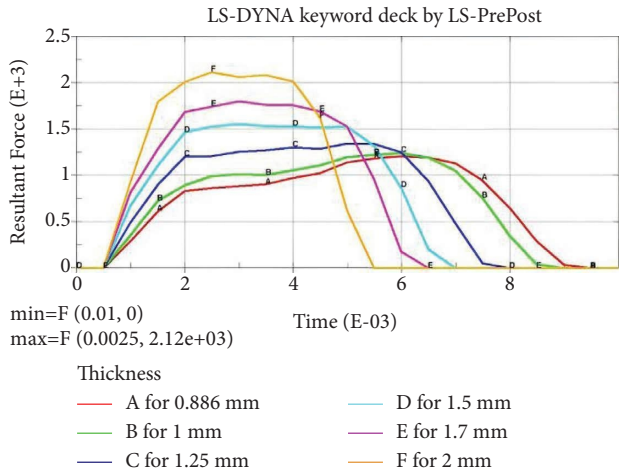

Figure 12: Impact force.

2.4. Effective von Moises Stress. At element 6255, the maximum stress value equals 0.8 GPa, as shown in Figure 13. Based on the material's mechanical properties, the steel material's strength and failure criteria are established. Based on the premise that no element dilatation was detected during the simulation, the beam is safe.

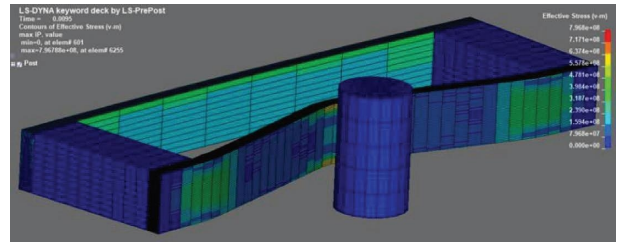

Figure 13: Von Mises stress.

2.5. Displacement. On the counter plot, the highest resulting deformation of the beam is depicted as 35 mm at node 3570. The amount of energy the beam can absorb depends on changes in its deformation. Figure 14 illustrates how, with this deformation, the incursion is very low and the force of impact is continuously increasing, but the damage will be less than with the preceding one (existing).

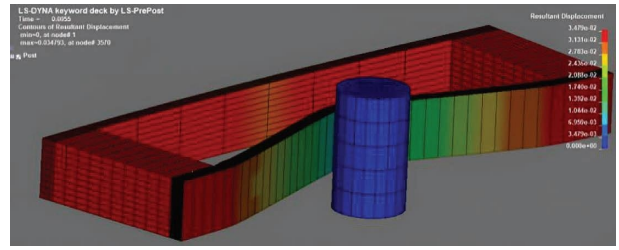

Figure 14: Resultant displacement.

2.6. Structural Response. Figure 15 displays the structural response of the present and modified BPV for 0.16 s.

The standard used to compare the structural reaction is the occupant's living space following impact. Figure 15(a) displays the remaining space for the current model, whereas Figure 15(b) displays the space for the updated model. The pole sticks out 539 millimeters in the case of an existing model, but only 377 millimeters in the case of a modified model. This demonstrates that the upgraded model maintained its larger living area after colliding with a side post.

2.7. Energy Absorption. Figure 16 displays the modified and original models' capacities for absorption. The total internal energy graph is used to compare the models' capacities for absorbing energy since identical circumstances are used in both models' simulations.

Green (modified) and red lines represent the internal energy of the model (existing). As seen in the graph, the modified model is the one that absorbs the most kinetic energy, with a value equivalent to 38.2 kJ of internal energy. The current model still has 35.3 kJ. This demonstrates that the redesigned model can absorb more kinetic energy under the same conditions with less distortion. This aids in lowering the amount of energy delivered to the BPV's occupants.

2.8. Verification Parameters. Without doing an experimental investigation, the verification method has the potential to check whether the results produced from computer simulations are adequate. Verification is possible in the case of LS-DYNA simulation [14, 18]. The most typical and sensible approaches are as follows:

(i) Energy ratio

(ii) TE/HE

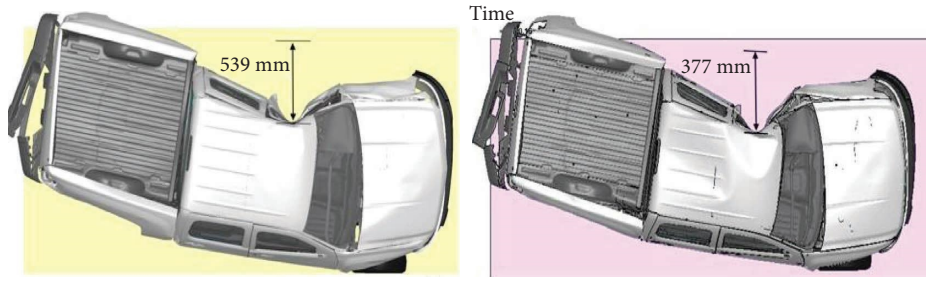

(a) (b)

Figure 15: Structural response of the existing and modified model.

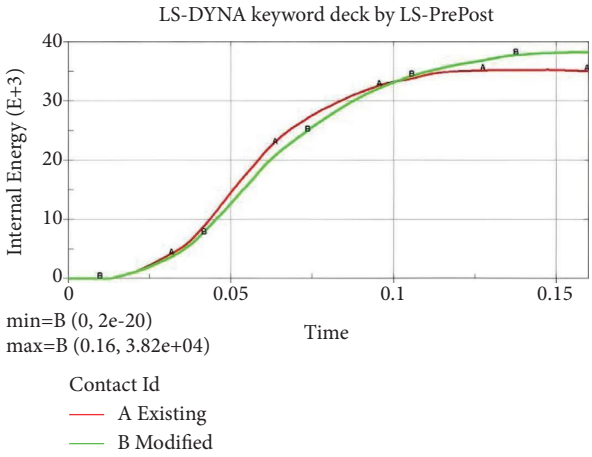

Figure 16: Energy absorbed.

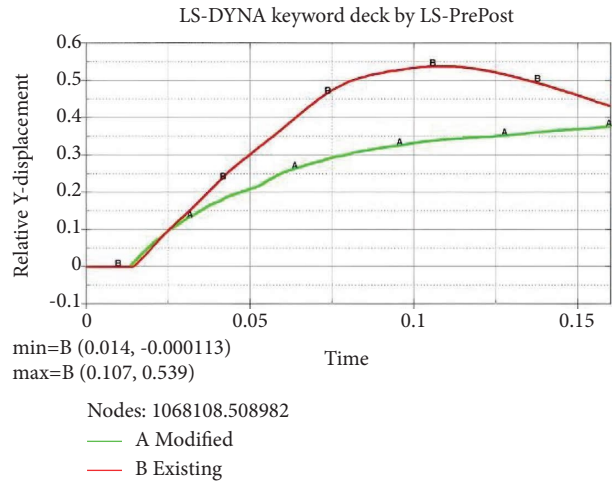

Figure 17: Deformation.

2.9. Deformation. The distortion brought on by the revised and current models is shown in Figure 17. The green line denotes the updated model, while the red line depicts the displacement of the original BPV. The old model's maximum deformation and the improved model's maximum deformation are 539 mm and 377 mm, respectively. It is obvious that the current model experiences the most distortion. This demonstrates that the updated model's 0.16-second length of intrusion to the occupant is reduced.

3. Ratio of Energy

As demonstrated in Figure 18, the energy ratio value ranges between 1 and 0.99975 for the 0.16 s simulation. Since the energy ratio result is within the range of 1.00 ± 0.07 [18], it is acceptable. The given value is so appropriate.

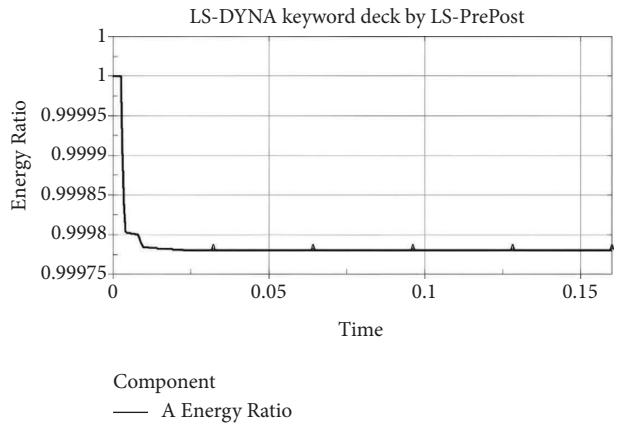

Figure 18: Energy ratio.

3.1. HE/TE. Another method for evaluating the finite element model's energy curves is to compare total energy to hourglass energy. A model with zero energy may result from hourglass energy.

If the energy in the hourglass makes up less than 5% of the total energy, the finite element model is accurate [18]. Figure 19 demonstrates that the ratio between the hourglass curve and the total energy curve is quite low—less than 5%.

3.1.1. Validation. Figure 20 shows the sequence of BPV side pole tests to validate with NCAP real-time tests. As shown in the figure, the FEM simulation is much similar to the real-time test. There is little difference on the side door glass; that

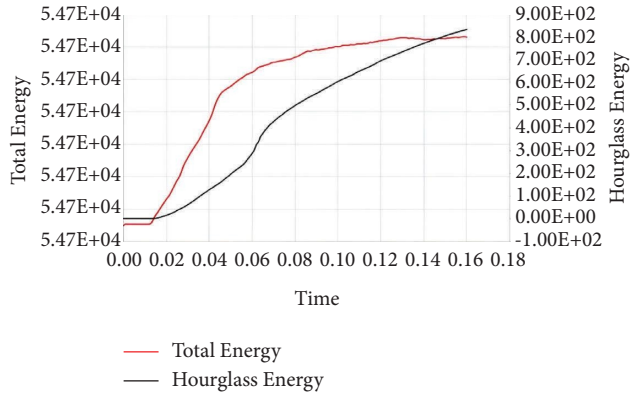

Figure 19: Hourglass energy to total energy.

Figure 20: Sequence of side pole crash FEA vs. real NCAP crash tests.

Table 5: Summary of the comparison between existing and modified models.

		Existing	Modified
For side beam test	Maximum deformation (mm)	36.1	27.6
	Maximum impact force (kN)	1.36	1.24
	Maximum internal energy (J)	25.8	27
Overall side crash	Maximum deformation (mm)	539	377
	Maximum impact force (kN)	84.6	72.4
	Maximum internal energy (kJ)	35.3	38.2

is, the property given in the FEM model is piecewise linear plasticity.

3.1.2. Summary of Comparison. Table 5 shows the result comparison between existing and modified vehicle models.

4. Conclusions

This study develops an FEA model of a Bishoftu pickup to improve the side crashworthiness of the current BPV using dynamic impact simulations. The modeling of BPV in the case of a side impact is clearly shown in the research. Therefore, crashworthiness is computationally analyzed using the current standards and laws. Additionally, an effort was made to change the BPV's structural crashworthiness based on the findings from the current model. The redesigned BPV now has better side crashworthiness characteristics as a consequence. The following is a summary of the major findings:

(i) The structure of the modified model has produced more living space than that of the existing model by only deforming 377 mm, whereas the existing model deformed 539 mm. This shows that in the event of a side collision, the modified model provides more protection to the occupants and the sensitive vehicle parts.

(ii) The impact force produced due to the collision of the vehicle with the pole is less for the modified model. A reduction of contact force implies that the transferred impact energy to the occupants is

reduced (minimized). So, a reduction of 12.2 kN (14.42%) of force was obtained by the implementation of the modifications.

(iii) The modified model also absorbs more kinetic energy than the existing model. It absorbed an additional 2.9 kJ of energy.

(iv) The change in mass between the old and the new material is 48.92 and 48.67 g, respectively; this shows that the fuel consumption is not affected by the optimization process due to the mass increase.

Data Availability

The data used to support the findings of this study are available from the corresponding author upon request.

Conflicts of Interest

The authors declare that there are no conflicts of interest.

References

[1] Who, *Global Status Report on Road Safety*, Road Safety Foundation, Geneva, 2018.

[2] V. H. Mohammad, "Evaluation of new steel and composite beam designs for side impact protection of a sedan as per fmvss 214, iihs and side Pole tests requirements," *Bachelor of Engineering*, Osmania University, China, 2010.

[3] E. Nassiopoulos and J. Njuguna, "Finite element dynamic simulation of whole rallying car structure: towards a better understanding of structural dynamics during side impacts," in *Proceedings of the 8th European LS-DYNA Users Conference*, Beijing China, May 2011.

[4] D. Wang, G. Dong, J. Zhang, and S. Huang, "Car side structure crashworthiness in pole and moving deformable barrier side impacts," *Tsinghua Science and Technology*, vol. 11, no. 6, pp. 725–730, 2006.

[5] P. S. Sa, G. Balaji, and K. Annamalai, "Numerical simulation of crashworthiness parameters for design optimization of an automotive crash-box," *International Journal for Simulation and Multidisciplinary Design Optimization*, vol. 13, p. 3, 2022.

[6] X. S. Gu, "A comparative study on multiobjective reliable and robust optimization for crashworthiness design of vehicle structure," *Structural and Multidisciplinary Optimization*, pp. 669–684, Springer, Berlin/Heidelberg, Germany, 2013.

[7] L. G. Yu, X. Gu, L. Qian, P. Jiang, W. Wang, and M. Yu, "Application of tailor rolled blanks in optimum design of pure electric vehicle crashworthiness and lightweight," *Thin-Walled Structures*, vol. 161, p. 107410, Article ID 107410, 2021.

[8] S. F. Abdulqadir and F. Tarlochan, "Composite hat structure design for vehicle safety: potential application to B-pillar and door intrusion beam," *Materials*, vol. 15, no. 3, p. 1084, 2022.

[9] P. P. Zhu, F. Pan, W. Chen, and F. A. Viana, "Lightweight design of vehicle parameters under crashworthiness using conservative surrogates," *Computers in Industry*, vol. 64, no. 3, pp. 280–289, 2013.

[10] A. Sheldon, "IIHS Side Impact Parametric Study Using LS DYNA® Reichert," in *Proceedings of the 15th International LS-DYNA® Users Conference*, NY China, June 2018.

[11] Nhtsa, "NHTSA crash test - consumer reports," *NHTSA crash test*, vol. 101, pp. 1–4, 2021.

[12] 2021 http://auto-che.com/v/dd/dd1022t-240-huanghai.html.

[13] Nhtsa. (n.d.), "Crash simulation vehicle models | NHTSA," 2022, https://www.nhtsa.gov/crash-simulation-vehicle-models.

[14] D. Hambissa, R. B. Nallamothu, and T. Andarge, "Analysis of three-wheeler vehicle structure at the event of side pole crash," *Journal of Engineering*, vol. 2022, pp. 1–13, Article ID 5490585, 2022.

[15] H. Singh and I. Edag, "Mass reduction for light-duty vehicles for model years 2017-2025 final Report," *Report No. DOT HS*, vol. 1, p. 582, 2012.

[16] Lstc, *Modeling of Composites in LS-DYNA*, Beijing, 2012, http://ftp.lstc.com/anonymous/outgoing/jday/composites/mat_comp.pdf.

[17] Y. Hu, C. Liu, J. Zhang, G. Ding, and Q. Wu, "Research on carbon-fiber-reinforced plastic bumper beam subjected to low-velocity frontal impact," *Advances in Mechanical Engineering*, vol. 7, no. 6, pp. 168781401558945–15, 2015.

[18] O. Gulavani, K. Hughes, and R. Vignjevic, "Explicit dynamic formulation to demonstrate compliance against quasi-static aircraft seat certification loads (CS25.561) -Part I: influence of time and mass scaling," *Proceedings of the Institution of Mechanical Engineers - Part G: Journal of Aerospace Engineering*, vol. 228, no. 11, pp. 1982–1995, 2014.